Electronic Supplementary Material (ESI) for Journal of Materials Chemistry A.
This journal is © The Royal Society of Chemistry 2022

Electronic Supplementary Information

An "Immobilizing and Relocating" Strategy for Highly Reversible Metallic Zinc Anode

Rui Yao, [a] Long Qian, [a] Guangyao Zhao, [a] Haojie Zhu, [a] Tingting Qin, [a] Chengxiang Xiao, [a] Hai Lin, [a] Feiyu Kang, [a] Chunyi Zhi [b] and Cheng Yang *[a]

[a.] Institute of Materials Research, Tsinghua Shenzhen International Graduate School, Tsinghua University, Shenzhen 518055, China.

[b.] Department of Materials Science and Engineering, City University of Hong Kong, 83 Tat Chee Avenue, Kowloon, Hong Kong SAR 999007, China.

E-mail: yang.cheng@sz.tsinghua.edu.cn

Experimental Section

Synthesis of δ-MnO_2

The δ-MnO_2 was fabricated using a facile hydrothermal method. The potassium permanganate and manganese sulfate powder (molar ratio 6:1) were dissolved in 30 mL of deionized water. Then the solution was sealed into a 50 mL Teflon-lined stainless-steel autoclave and heated at 160℃ for 12 h. After the solution was cooled to room temperature, it was washed with deionized water and centrifuged three times, then freeze-drying for 24 h to obtain the final product. The activated carbon (AC) was a commercial powder used without further purification.

Preparation of Electrolytes and Electrodes and Fabrication of Cells

Hydrated zinc sulfate ($ZnSO_4 \cdot 7H_2O$) and betaine were all purchased from Alfa Aesar. The baseline electrolyte was prepared by dissolving 2 M $ZnSO_4 \cdot 7H_2O$ into the deionized water marked as ZS. The modified electrolytes were prepared by dissolving 10 mM, 50 mM, 100 mM, 500 mM betaine, and 2 M $ZnSO_4 \cdot 7H_2O$ into the deionized water, marked as 10 mM B-ZS, 50 mM B-ZS, 100 mM B-ZS and 500 mM B-ZS, respectively. The δ-MnO_2 cathode was fabricated by mixing the δ-MnO_2 active materials with Super P and polyvinylidene fluoride (PVDF) at the weight ratio of 8:1:1. The above mixture was mixed with an appropriate amount of N-methyl-2-pyrrolidone (NMP) to form a slurry. The slurry was stirred vigorously for 4 h and spread onto titanium foil. Then it was dried in a vacuum oven at 60℃ overnight. The mass loading of δ-MnO_2 in galvanostatic cycling was 2.0 mg cm^{-2}-2.2 mg cm^{-2}. CR2032-type coin-cells were assembled in an air atmosphere, using zinc foil (thickness 80 μm and 20 μm) as the anode and glass fiber filter (Whatman, grade GF/A) as the separator.

The preparation process of the AC cathode is consistent with that of the δ-MnO_2 cathode. The mass loading of AC in galvanostatic cycling was 1.1 mg cm^{-2}-1.3 mg cm^{-2}.

Electrochemical Tests

The cyclic voltammetry (CV), the linear scanning voltammetry (LSV), the electrochemical impedance spectroscopy (EIS), and the linear polarization curve were conducted using a Bio-Logic electrochemical workstation (VMP-300). The transfer number test was performed using Princeton Applied Research electrochemical workstation (PARSTAT 4000A). Galvanostatic cycling, rate capability, and shelf life were tested with LAND testing systems. The cycled Zn||Zn symmetric cells were obtained after 30 cycles at the current density of 1 mA cm^{-2} and the areal capacity of 0.5 mAh cm^{-2} in different electrolytes. The cycled electrodes were obtained by disassembling Zn||Zn symmetric cells after 30 cycles at the current density of 1 mA cm^{-2} and the areal capacity of 0.5 mAh cm^{-2} in different electrolytes. Two and three electrodes were performed in the atmosphere, and a 50 mL electrolytic cell was used as the testing vessel.

Materials Characterizations

Scanning electron microscopy (SEM, Hitachi SU8010, Japan) was performed to observe the morphology and microstructure on the electrode surface. X-ray diffraction (XRD, D8 Advance, Germany) with Cu-Kα1 radiation (λ=1.5405 Å) was performed to identify the components on the electrode surface. The conductivity meter (Mettler Toledo FE38, Swiss) and rotational viscometer (NDJ-79, China) were adopted to measure the physicochemical properties of electrolytes. Differential scanning calorimetry (DSC, Mettler Toledo, Swiss) was adopted to analyze the changes in phase-transition temperature in different electrolytes,

and samples were scanned from -60℃ to 30℃ at a rate of 5℃ min^{-1} under nitrogen atmosphere. Fourier transform infrared spectrometer (Nicolet IS50, America) in the wavenumber range of 400 cm^{-1}~4000 cm^{-1} was adopted to obtain the attenuated total reflectance (ATR) infrared spectrum of electrolytes. Nuclear magnetic resonance spectrum (NMR, Bruker AVANCE III 400, Germany) was adopted to analyze interactions between electrolyte components. High-resolution mass spectroscopy (HRMS, Q exactive Focus, America) was adopted to confirm electrolyte components.

DFT Calculations

First-principles calculations are performed based on density-functional theory (DFT) by using Vienna Ab initio Simulation Package (VASP) with the projector augmented wave (PAW) method. The cutoff kinetic energy of 400 eV is chosen for the plane wave basis. We employ the Perdew-Burke-Ernzerhof (PBE) functional with generalized gradient approximation (GGA) for the exchange-correlation energy. According to the X-ray diffraction patterns of adopted metallic zinc in the current work, the Zn (101) surface plane shows the highest peak intensity. Therefore, it is adopted as the representative surface plane for DFT calculations. For the Zn (101) surface containing 4 atomic layers, a vacuum thickness of 15 Å in two aperiodic directions is used to eliminate the interactions between neighboring layers. Based on the test of convergence accuracy, we use (2×2×1) Monkhorst-Pack k-point mesh to represent the reciprocal space of the unit cell. The crystal structure is fully optimized using the conjugated gradient algorithm, and the convergence criteria for energy and force are set to 10^{-4} eV and 0.01 eV $Å^{-1}$, respectively.

COMSOL multiphysics simulations

The transient simulation model was carried out on COMSOL Multiphysics software using the physics module of "Tertiary current density" with the Nernst-Planck transport equation. Here, the ion transport in the electrolyte region is dominated by molecular diffusion and electromigration, where the governing equation for ion transport is depicted by:

$$\frac{\partial c_i}{\partial t} = \nabla \cdot \left(D_i \nabla c_i + z_i \frac{D_i}{RT} F c_i \nabla \varphi_l \right) \quad \text{Eq. 1}$$

The electrochemical reaction is applied at the electrode surface with protrusion configurations, and the electrochemical reaction rate is determined by the local ion concentration and the corresponding overpotential:

$$i = i_0 \frac{c_i \ F\eta}{c_{ref} RT} \quad \text{Eq. 2}$$

Accordingly, the ions concentration reaction rate is solved by:

$$R_i = - \frac{v_i i}{z_i F} \quad \text{Eq. 3}$$

Table S1. Physical meanings and units represented by different abbreviations.

Abbreviation	Physical meanings	Units
i	Ion current density	A m^{-2}
D_i	i ions diffusion coefficient	m^2 s^{-1}
c_i	i ions local concentration	mol m^{-3}
z_i	i ions charge number	-
φ_l	Electrolyte potential	V
i_0	Reference current density	1000 A m^{-2}
c_{ref}	i ions reference concentration	1 mol L^{-1}
v_i	Electrochemical stoichiometric number for i ions	-
η	Overpotential; $\eta=\varphi_s-\varphi_l$; φ_s: electrode potential	V

Table S2. Performance comparison of the electrochemical reversibility in half cells.

Average CE	Cycle No.	Current density and areal capacity	Reference
99.93%	2210	1 mA cm^{-2}, 0.5 mAh cm^{-2}	This work
99.50%	230	1 mA cm^{-2}, 1 mAh cm^{-2}	Chem Eng J., 2023, 452, 139577
99.72%	1000	0.5 mA cm^{-2}, 0.5 mAh cm^{-2}	Nano Lett., 2022, 22, 7535
99.70%	1000	1 mA cm^{-2}, 0.5 mAh cm^{-2}	Adv. Energy Mater., 2022, 12, 2103231
99.06%	200	1 mA cm^{-2}, 1 mAh cm^{-2}	Adv. Mater., 2022, n/a, 2207344
99.60%	300	0.5 mA cm^{-2}, 0.25 mAh cm^{-2}	Adv. Mater., 2022, 34, 2203710
99.50%	1000	1 mA cm^{-2}, 1 mAh cm^{-2}	Energy Environ. Sci., 2021, 14, 5947
99.40%	400	1 mA cm^{-2}, 0.5 mAh cm^{-2}	Adv. Mater., 2021, 33, 2007416
99.40%	400	1 mA cm^{-2}, 0.5 mAh cm^{-2}	Nat. Sustain., 2021, 5, 205

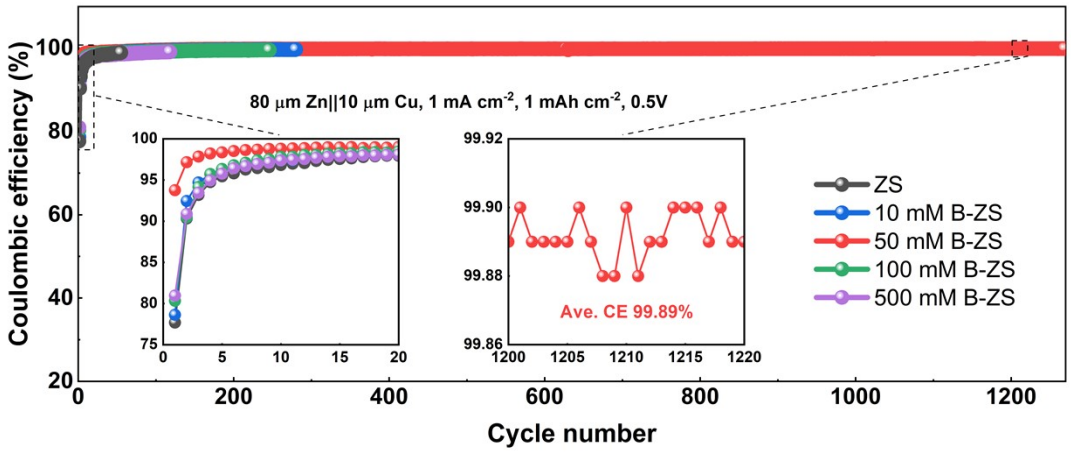

Fig. S1 Electrochemical reversibility test of zinc plating/stripping in Zn||Cu half-cells.

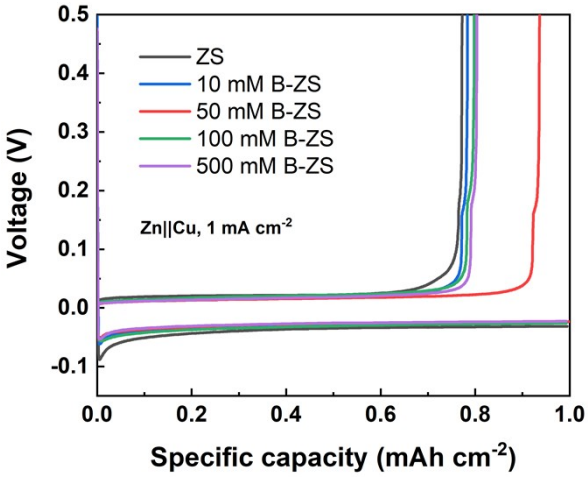

Fig. S2 Charge and discharge curves ast initial cycles.

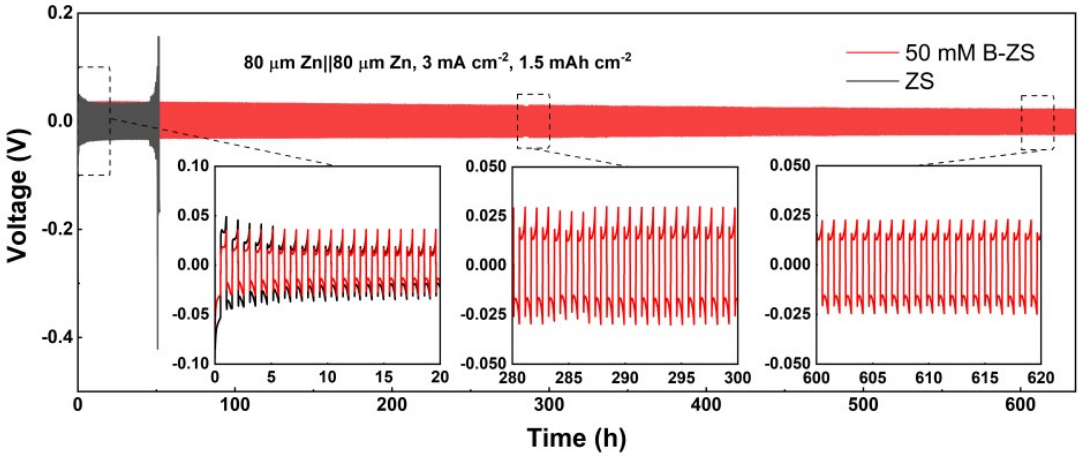

Fig. S3 Galvanostatic zinc plating/stripping in Zn||Zn symmetric cells.

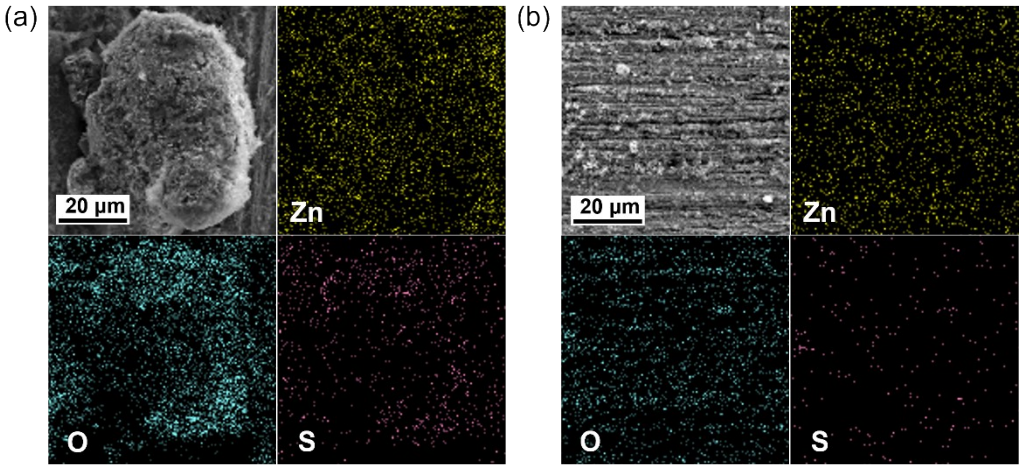

Fig. S4 Energy dispersive spectroscopy of cycled electrodes in (a) ZS baseline electrolyte and (b) 50 mM B-ZS modified electrolyte.

To obtain cleaner results of EDS mapping, the tested voltage was increased from 5 kV to 15 kV.

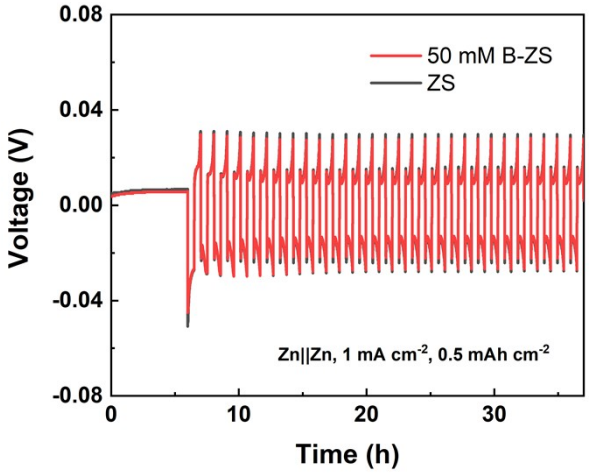

Fig. S5 The voltage-time curves during precycling of Zn||Zn symmetric cells.

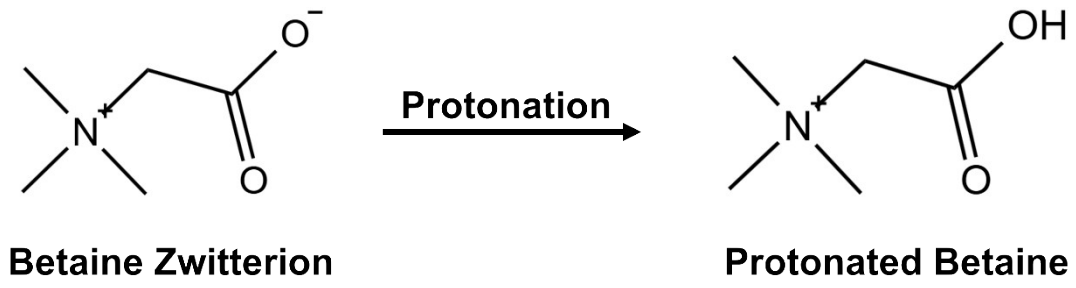

Fig. S6 Structure diagram of the betaine zwitterion before and after protonation.

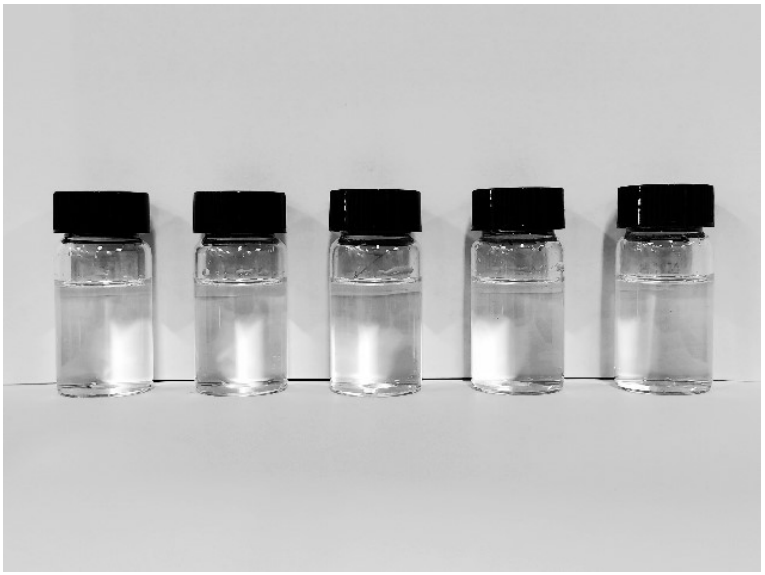

Fig. S7 Optical images of electrolytes (From left to right, ZS, 10 mM B-ZS, 50 mM B-ZS, 100 mM B-ZS, 500 mM B-ZS electrolyte, respectively).

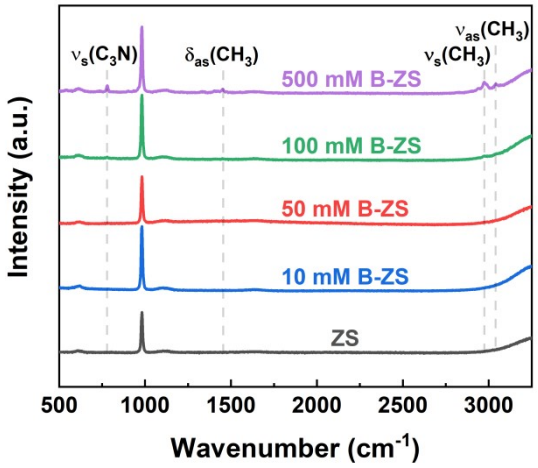

Fig. S8 Raman spectroscopy of electrolytes.

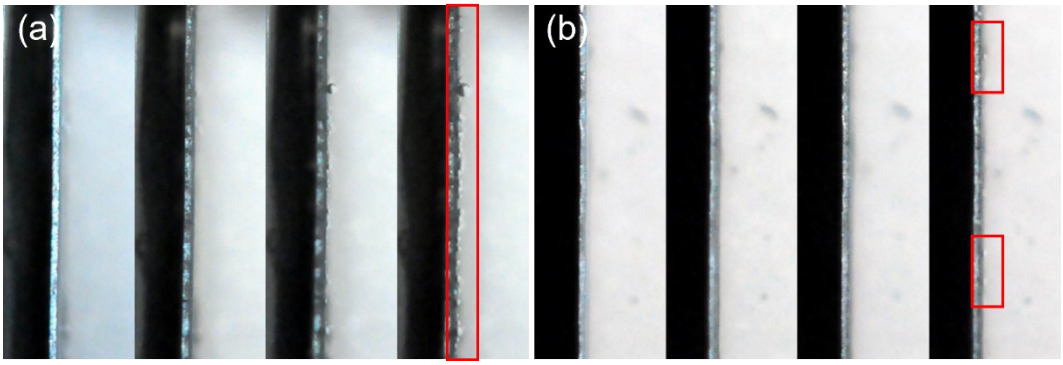

Fig. S9 In-situ optical images of zinc plating in (a) ZS baseline electrolyte and (b) 50 mM B-ZS modified electrolyte at the current density of 3 mA cm^{-2} (From left to right, the images at the 0 mins, 10 mins, 20mins and 30mins, respectively).

As shown in marked areas, in-situ optical images of zinc plating in the ZS baseline electrolyte show a lot of bubbles. And the in-situ optical images of zinc plating in 50 mM B-ZS modified electrolyte show fewer bubbles. It indicates that the introduction of betaine zwitterions can effectively inhibit hydrogen evolution during zinc plating.

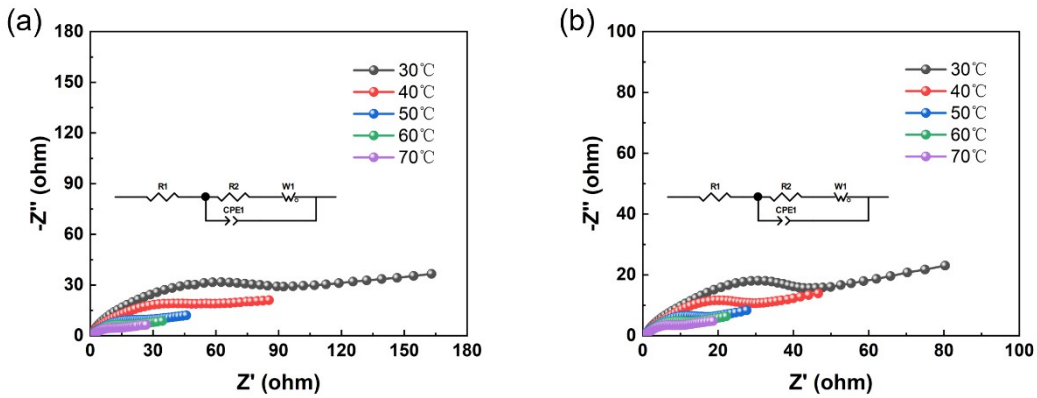

Fig. S10 Electrochemical impedance spectroscopy of Zn||Zn symmetric cells with (a) ZS baseline electrolyte and (b) 50 mM B-ZS modified electrolyte.

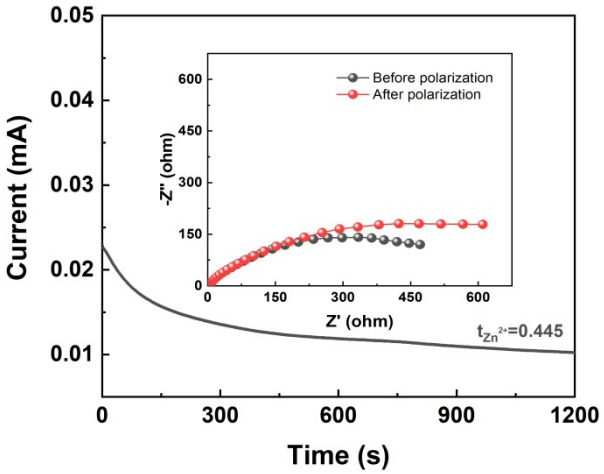

Fig. S11 Transfer number test in ZS baseline electrolyte.

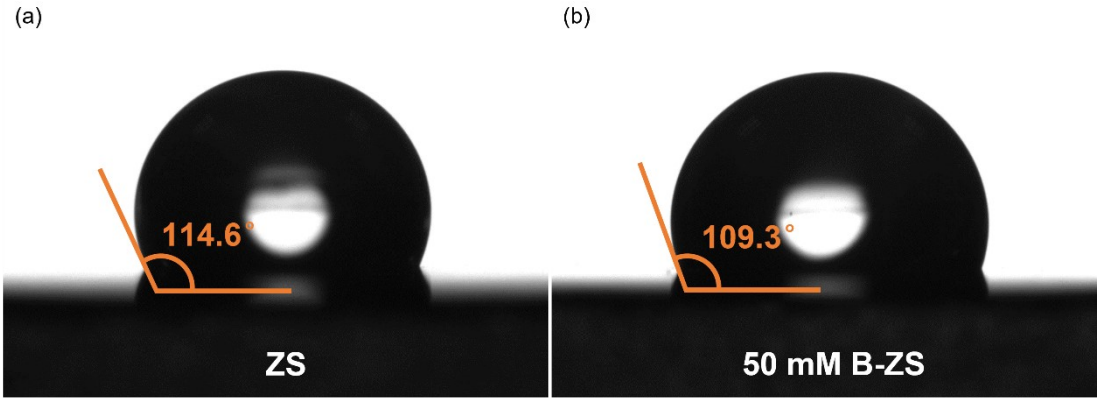

Fig. S12 Contact angle tests of (a) ZS baseline electrolyte and (b) 50 mM B-ZS modified electrolyte on metallic zinc.

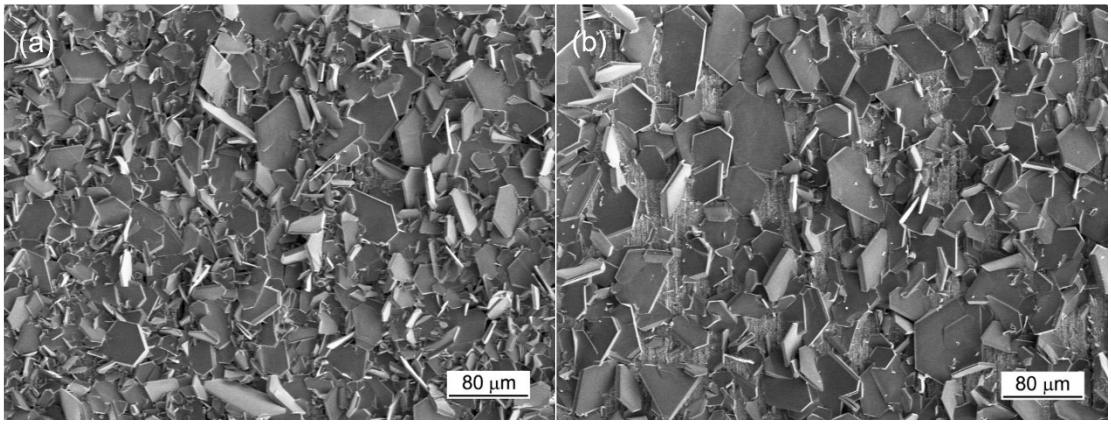

Fig. S13 SEM of soaked metallic zinc in (a) ZS baseline electrolyte and (b) 50 mM B-ZS electrolyte.

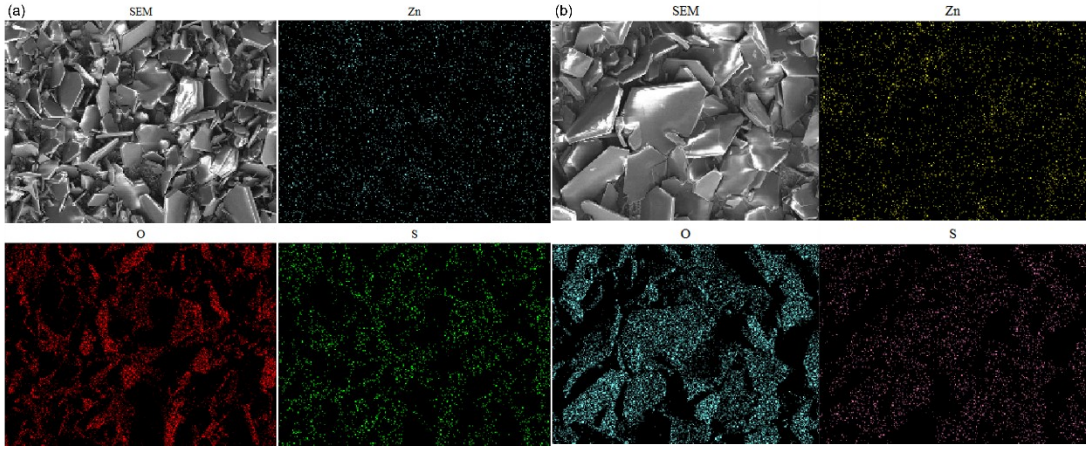

Fig. S14 EDS mapping of soaked metallic zinc in (a) ZS baseline electrolytes and (b) 50 mM BZS modified electrolyte.

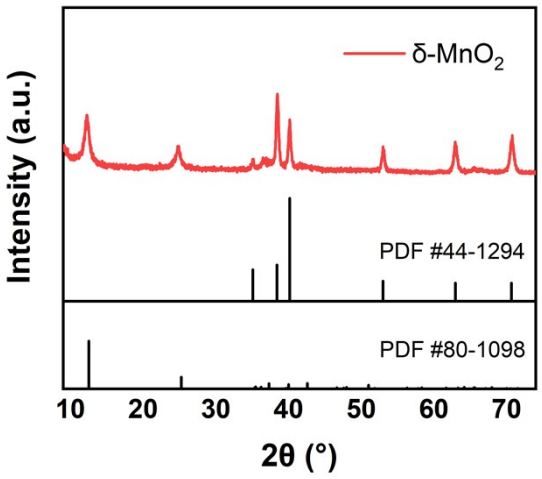

Fig. S15 XRD patterns of MnO_2 electrodes.

MnO_2 active materials (PDF #80-1098)[1] were spread on the Ti substrate (PDF #44-1294).

1. D. Wang, L. Wang, G. Liang, H. Li, Z. Liu, Z. Tang, J. Liang and C. Zhi, *ACS Nano*, 2019, 13, 10643.

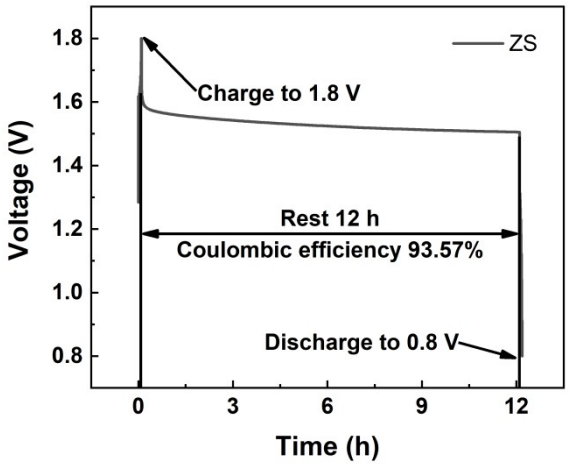

Fig. S16 Voltage-time curves of full-cells with ZS baseline electrolyte.

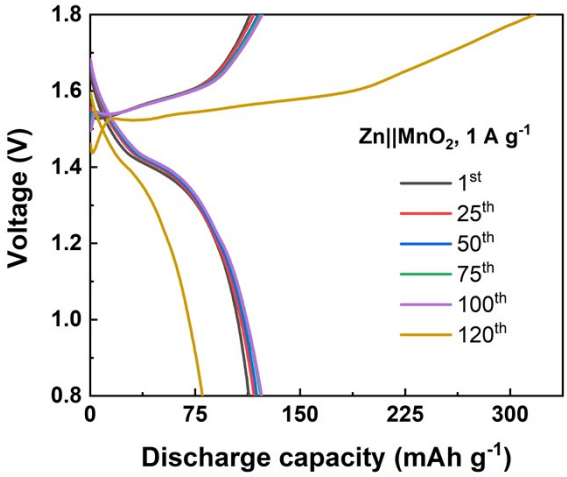

Fig. S17 Charge and discharge curves of full-cells with ZS baseline electrolyte.

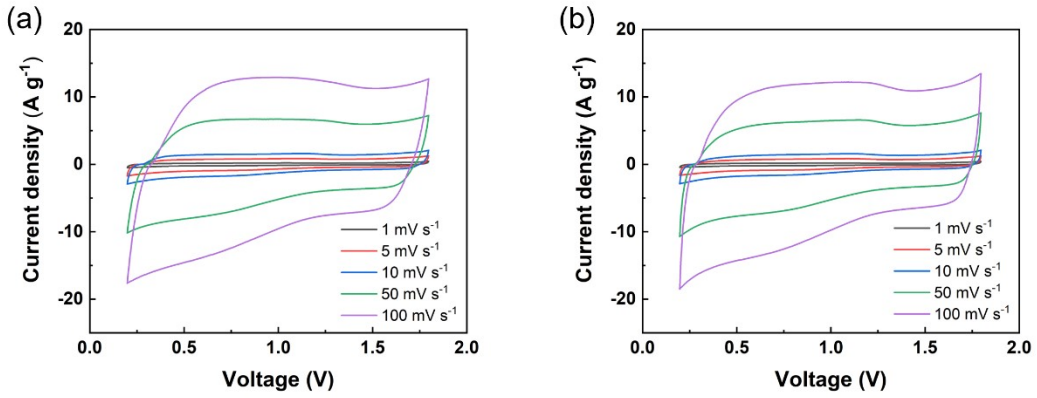

Fig. S18 Cyclic Voltammetry curves of Zn||AC hybrid capacitors with (a) ZS baseline electrolyte and (b) 50 mM B-ZS modified electrolyte.

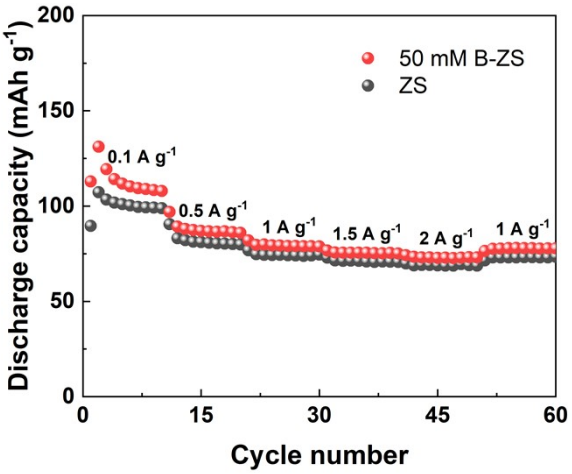

Fig. S19 Rate capability of Zn||AC hybrid capacitors.

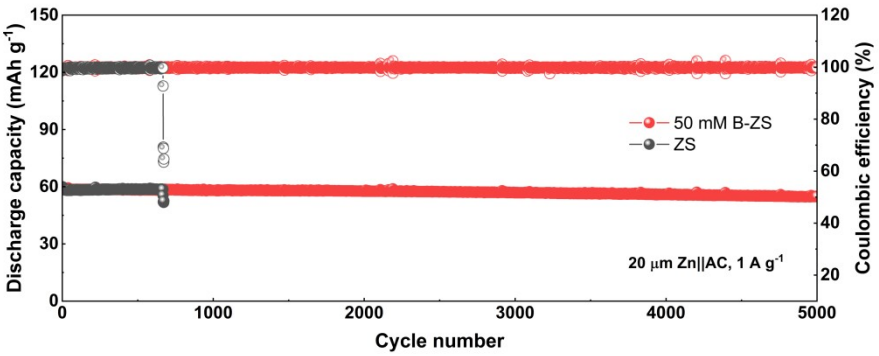

Fig. S20 Galvanostatic cycling of Zn||AC hybrid capacitors.

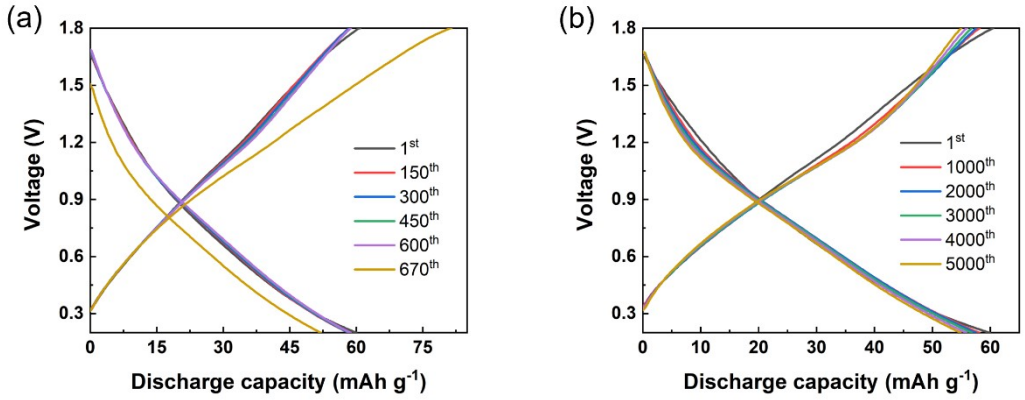

Fig. S21 Charge and discharge curves of Zn||AC hybrid capacitors with (a) ZS baseline electrolyte and (b) 50 mM B-ZS modified electrolyte.